$LaVO_3$: A true Kugel-Khomskii system

Xue-Jing Zhang,[1] Erik Koch,[1,2] and Eva Pavarini[1,2]
[1]*Institute for Advanced Simulation, Forschungszentrum Jülich, 52425 Jülich, Germany*
[2]*JARA High-Performance Computing, 52062, Aachen, Germany.*

(Received 1 February 2022; revised 24 August 2022; accepted 25 August 2022; published 8 September 2022)

We show that the t_{2g}^2 perovskite $LaVO_3$, in its orthorhombic phase, is a rare case of a system hosting an orbital-ordering Kugel'-Khomskii phase transition rather than being controlled by the Coulomb-enhanced crystal-field splitting. We find that, as a consequence of this, the magnetic transition is close to (and even above) the superexchange driven orbital-ordering transition, whereas typically magnetism arises at much lower temperatures than orbital ordering. Our results support the experimental scenario of orbital ordering and *G*-type spin correlations just above the monoclinic-to-orthorhombic structural change. To explore the effects of crystal-field splitting and filling, we compare to YVO_3 and t_{2g}^1 titanates. In all these materials the crystal field is sufficiently large to suppress the Kugel'-Khomskii phase transition.

DOI: 10.1103/PhysRevB.106.115110

I. INTRODUCTION

Almost 50 years ago, Kugel' and Khomskii (KK) showed in a classic paper that, in strongly correlated materials, orbital ordering (OO) can arise from pure superexchange (SE) interactions [1]. It can, however, also result from the crystal-field (CF) splitting via a lattice distortion, i.e., from electron-lattice coupling [2]. In typical cases both mechanisms lead to similar types of ordering so that identifying which one actually drives the transition is a "chicken-and-egg problem" [3]. Despite the intensive search, it has, therefore, been hard to find an undisputed realization of a KK system.

Initially it was believed that the e_g perovskites $KCuF_3$ and $LaMnO_3$ could be KK materials [3–6]. In recent years, however, it was proven that neither in these, nor in other e_g systems, superexchange interactions are strong enough to drive the OO transition alone [7–12]. In fact, in order to explain the presence of OO at high temperature, lattice distortions, arising from the Jahn-Teller effect, the Born-Meyer potential, or both [13], have to be present. The CF splitting generated by the distortions is then effectively enhanced by the Coulomb repulsion, which suppresses orbital fluctuations [14–16], leading to a very robust OO state. The actual form of the ordered state is then essentially determined by the crystal field. Recently, the case of t_{2g}^1 perovskites was explored as possible alternative [17]. In fact, the CF is typically weaker in π-bond than in σ-bond materials, whereas, at the same time, the orbital degeneracy is larger. This can potentially turn the balance of interactions in favor of SE. It was indeed shown that $T_{\rm KK}$, the critical temperature of super-exchange-driven orbital ordering, is remarkably large in $LaTiO_3$ and $YTiO_3$, about 300 K [17]. At the same time it became, however, also clear that even in these systems OO is dominated by correlation-enhanced CF splitting rather than the SE interaction.

In this paper we identify the first compound in which KK multiorbital superexchange yields an orbital-ordering phase transition at observable temperatures: the t_{2g}^2 perovskite $LaVO_3$ in its orthorhombic ($GdFeO_3$-type structure) phase. $LaVO_3$ has drawn a lot of attention due to its peculiar properties and phase diagram [18–24]. In the low-temperature monoclinic phase ($T < T_{\rm str} \sim 140$ K), it exhibits a *C*-type magnetic structure. Due to the small distortions of the VO_6 octahedra, it was suggested that *C*-type spin order could arise from strong xz/yz orbital fluctuations [25]. Calculations accounting for the $GdFeO_3$-type distortions have, however, shown that orbital fluctuations are suppressed below $T_{\rm str}$, and classical OO is sufficient to explain *C*-type spin order [16]. The debate remains open for what concerns the intriguing phase just above the structural phase-transition, $T_{\rm str} < T < T_{\rm N'} \sim 145$ K. Here thermodynamic anomalies and weak magnetic peaks suggest a change in spin-orbital order, either long or short ranged [22–24], the origin of which is, however, unclear. Our results show that the KK nature of $LaVO_3$ provides a natural explanation.

To understand what makes orthorhombic $LaVO_3$ special, we compare it with the similar but more distorted YVO_3 and the two isostructural t_{2g}^1 titanates. We start from the paramagnetic (PM) phase. We show that, for the vanadates, $T_{\rm KK}$ is actually smaller than for titanates, $T_{\rm KK} \sim 190$ K in $LaVO_3$ and $T_{\rm KK} \sim 150$ K in YVO_3, but at the same time the crystal field is weaker, for $LaVO_3$ more so than for YVO_3. The surprising result of the energy-scale balance is that, while in YVO_3 the occupied state is still, to a large extent, determined by the CF splitting, for $LaVO_3$ it substantially differs from CF-based predictions (Fig. 1). Staying with $LaVO_3$, we find that the actual orbital-ordering temperature $T_{\rm OO}$ is close to $T_{\rm KK}$. Even more remarkable is the outcome of magnetic calculations. They yield a *G*-type antiferromagnetic (AF) phase with $T_N > T_{\rm OO} \sim T_{\rm KK} > T_{\rm str}$. This is opposite to what typically happens

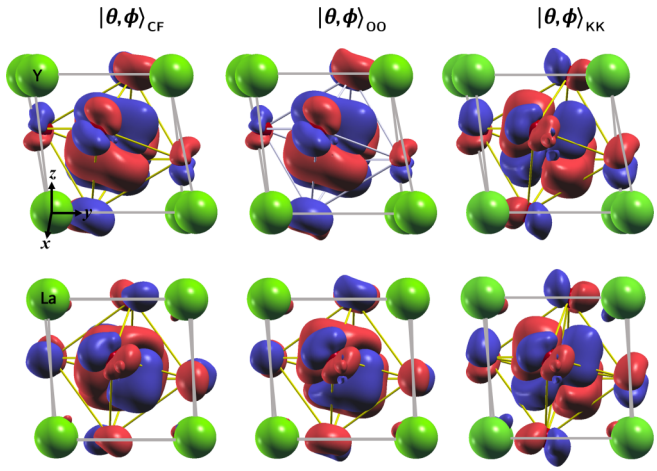

FIG. 1. Left: LDA, highest-energy CF state $|\theta,\phi\rangle_{\rm CF}$. Center and right: dynamical-mean-field theory (DMFT) hole orbital at 90 K. $|\theta,\phi\rangle_{\rm OO}$: experimental structure. $|\theta,\phi\rangle_{\rm KK}$: idealized case with no CF splitting. Top line: YVO_3. Bottom line: $LaVO_3$.

in orbitally ordered materials in which T_N is smaller than $T_{\rm OO}$, often sizably so. Our results provide a microscopic explanation of the spin-orbital correlations found right above $T_{\rm str}$ in experiments [22–24].

II. ORBITAL-ORDERING TRANSITION

In order to determine the onset of the super-exchange-driven orbital-ordering transition $T_{\rm KK}$, we adopt the approach pioneered in Refs. [7,8]. It consists in progressively reducing the static CF splitting to single out the effects of pure superexchange from those of Coulomb-enhanced structural distortions. Calculations are performed using the local-density approximation plus dynamical-mean-field theory method (LDA+DMFT) [26] for the materials-specific t_{2g} Hubbard model,

$$\hat{H} = -\sum_{ii'\sigma}\sum_{mm'} t^{i,i'}_{mm'} c^{\dagger}_{im\sigma} c_{i'm'\sigma} + U\sum_{im}\hat{n}_{im\uparrow}\hat{n}_{im\downarrow} + \frac{1}{2}\sum_{i\sigma\sigma'}\sum_{m\neq m'}(U-2J-J\delta_{\sigma,\sigma'})\hat{n}_{im\sigma}\hat{n}_{im'\sigma'} - J\sum_{im\neq m'}(c^{\dagger}_{im\uparrow}c^{\dagger}_{im\downarrow}c_{im'\uparrow}c_{im'\downarrow} + c^{\dagger}_{im\uparrow}c_{im\downarrow}c^{\dagger}_{im'\downarrow}c_{im'\uparrow}). \quad (1)$$

Here $-t^{i,i'}_{mm'}$ $(i \neq i')$ are the LDA hopping integrals [27] from orbital m on site i to orbital m' on site i'. They are obtained in a localized Wannier function basis via the linearized augmented plane-wave method [28–30]. The operator $c^{\dagger}_{im\sigma}$ ($c_{im\sigma}$) creates (annihilates) an electron with spin σ in Wannier state m at site i, and $n_{im\sigma} = c^{\dagger}_{im\sigma}c_{im\sigma}$. For the screened Coulomb parameters we use values established in previous works [14–16,31]: U=5 eV with J=0.68 eV for YVO_3 and $LaVO_3$ and J=0.64 eV for $YTiO_3$ and $LaTiO_3$. We then solve this model using DMFT. The quantum impurity solver is the generalized hybridization-expansion continuous-time quantum Monte Carlo method [32] in the implementation of Refs. [10,12,33].

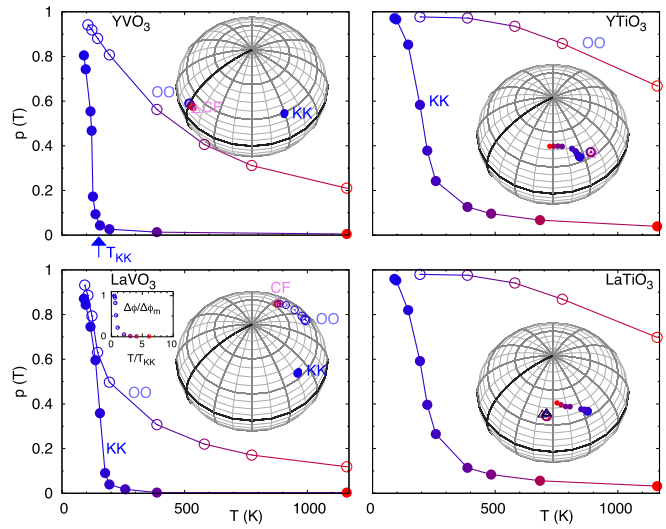

FIG. 2. Lines: Orbital polarization $p(T)$, defined as $p(T)=(-1)^n((n_1+n_2)/2-n_3)$, as a function of temperature T; here n_i is the occupation of natural orbitals with $n_{i+1}<n_i$ for n=2 and $n_{i+1}>n_i$ for n=1. Bloch spheres: angles defining the least (n=2) or most (n=1) occupied orbital, $|\theta,\phi\rangle = \sin\theta\,\cos\phi|xz\rangle + \cos\theta|xy\rangle + \sin\theta\,\sin\phi|yz\rangle$. Empty circles (OO): experimental structure. Filled circles (KK): Idealized case with no CF splitting. Triangles (CF): crystal-field orbital. Left: vanadates. Right: titanates. Equatorial line: θ=90°. Thick-line meridian: ϕ=0°. The equivalent solution at $|\pi-\theta,\phi+\pi\rangle$ is on the far side of the sphere. For $LaVO_3$, an inset shows explicitly the sudden variation of ϕ across $T_{\rm KK}$; $\Delta\phi = \phi - \phi_{\rm CF}$ is the difference with respect to the CF value of ϕ.

The main results are summarized in Fig. 2. We start from the experimental structure with full CF splitting (empty circles). For the titanates, the orbital polarization $p_{\rm OO}(T)$ is already very large at 1000 K; instead, in the vanadates, and $LaVO_3$ in particular, $p_{\rm OO}(T) \longrightarrow 1$ at much lower temperatures [16]. The OO ground state, for the t^2_{2g} case, is characterized, at a given site, by the least occupied (or hole) natural orbital,

$$|\theta,\phi\rangle = \sin\theta\,\cos\phi|xz\rangle + \cos\theta|xy\rangle + \sin\theta\,\sin\phi|yz\rangle, \quad (2)$$

represented via open circles on the Bloch spheres in the figure. The hole orbitals at the neighboring sites, yielding the spatial arrangement of orbitals, can be obtained from (2) using symmetries [34]. For t^1_{2g} systems, (2) represents the most occupied orbital. As the figure shows, in the t^1_{2g} case, at any temperature $|\theta,\phi\rangle_{\rm OO}$ is very close to $|\theta,\phi\rangle_{\rm CF}$, the lowest energy crystal-field orbital (open triangle). Switching to t^2_{2g} systems, for YVO_3, the hole orbital is $|\theta,\phi\rangle_{\rm OO} \sim |72°,-1°\rangle$, quite close to the crystal-field state with the highest-energy $|\theta,\phi\rangle_{\rm CF} \sim |71°,9°\rangle$. Up to here, the results conform to the established picture: The CF splitting, enhanced by Coulomb repulsion, determines the shape of the ordered state [7–12].

The conclusion changes dramatically as soon as we turn to $LaVO_3$. Here, $p_{\rm OO}(T)$ has a sharp turn upwards at $T_{\rm KK} \sim T_{\rm OO} \sim 190$ K. Furthermore, lowering the temperature, the hole orbital $|\theta,\phi\rangle_{\rm OO}$ turns markedly away from the CF high-energy state $|\theta,\phi\rangle_{\rm CF} \sim |142°,25°\rangle$, showing that the

ordering mechanism works against the crystal-field splitting. At the lowest temperature we could reach numerically $|\theta, \phi\rangle_{OO} \sim |130°, -8°\rangle$. This can be seen on the Bloch sphere, where the empty circles move away from the triangle as well as in the inset showing the sudden variation of the most occupied orbital across T_{KK}.

Next we analyze the results in the zero CF splitting limit, which yields the pure Kugel'-Khomskii transition. The results are shown as filled circles in Fig. 2, and the orbital polarization curve is $p_{KK}(T)$. For the titanates, $p_{KK}(T)$ exhibits a small tail at high temperature and then sharply rises at $T_{KK} \sim 300$ K; at this transition $p_{OO}(T)$ has, however, long saturated. For the vanadates the rise in $p_{KK}(T)$ is much sharper, and at a markedly lower temperature, $T_{KK} \sim 150$ K in YVO_3 and $T_{KK} \sim 190$ K in $LaVO_3$, whereas the high-temperature tail is virtually absent. Furthermore, for $LaVO_3$, the figure shows that $p_{OO}(T) \sim p_{KK}(T)$ for temperatures sufficiently below $T_{KK} \sim T_{OO}$. At the same time, decreasing the temperature, the OO hole orbital for the experimental structure (empty circles), rapidly moves towards the KK hole (filled circles). These results together identify $LaVO_3$ as the best known representation of a Kugel'-Khomskii system, i.e., a system hosting an orbital-ordering KK-driven phase transition. The KK superexchange interaction both determines the value of $T_{KK} \sim T_{OO}$ and pulls the hole away from the crystal-field orbital towards the KK orbital. YVO_3 is on the borderline but still on the side where the Coulomb-enhanced CF interaction dominates; that means, the hole stays close to the crystal-field orbital even below T_{OO}. Furthermore, for YVO_3, the critical temperature $T_{KK} \sim 150$ K itself is smaller than the $T_{str} \sim 200$ K, the temperature at which the orthorhombic-to-monoclinic phase transition occurs. For $LaVO_3$ the opposite is true ($T_{KK} \sim T_{OO} > T_{str}$).

III. SUPEREXCHANGE HAMILTONIAN AND ENERGY SURFACES

Further support for these conclusions comes from the analysis of superexchange energy-gain surfaces, Fig. 3. We obtain them adopting the approach recently introduced in Refs. [17,35], representing the multiorbital KK superexchange Hamiltonian via its irreducible-tensor decomposition,

$$\hat{H}_{SE} = \frac{1}{2} \sum_{i,j} \sum_{\mu\mu'} \sum_{r,r'} \hat{\tau}_i^{r,\mu;qv} D_{r\mu,r'\mu'}^{ij;qv} \hat{\tau}_j^{r',\mu';qv} \delta_{q,0} \delta_{v,0}. \quad (3)$$

Here $r = 0$–2 is the orbital rank, μ is the associated components, and the spin rank is q with components v. The analytic expressions of the tensor elements can be found in Refs. [17,35]. The terms with $q = q' = 0$ and $r = 0$, $r' \neq 0$ (or vice versa) describe the (linear) orbital Zeeman interaction [12]. These contributions behave as a site-dependent crystal-field splitting since the $r = q = 0$ tensor operator only counts the number of electrons on the neighboring site, here $n = 2$. The $r \neq 0$, $r' \neq 0$ quadratic terms are those that can actually lead to a phase transition. Terms with $q = 0$ are purely paramagnetic, those with $r = 0$ purely paraorbital. In Fig. 3 we show results for the *ab initio* hopping integrals and, for reference, an idealized cubic case. Comparing the results for the PM phase with those in Fig. 2, one may see that the angles θ_M, ϕ_M

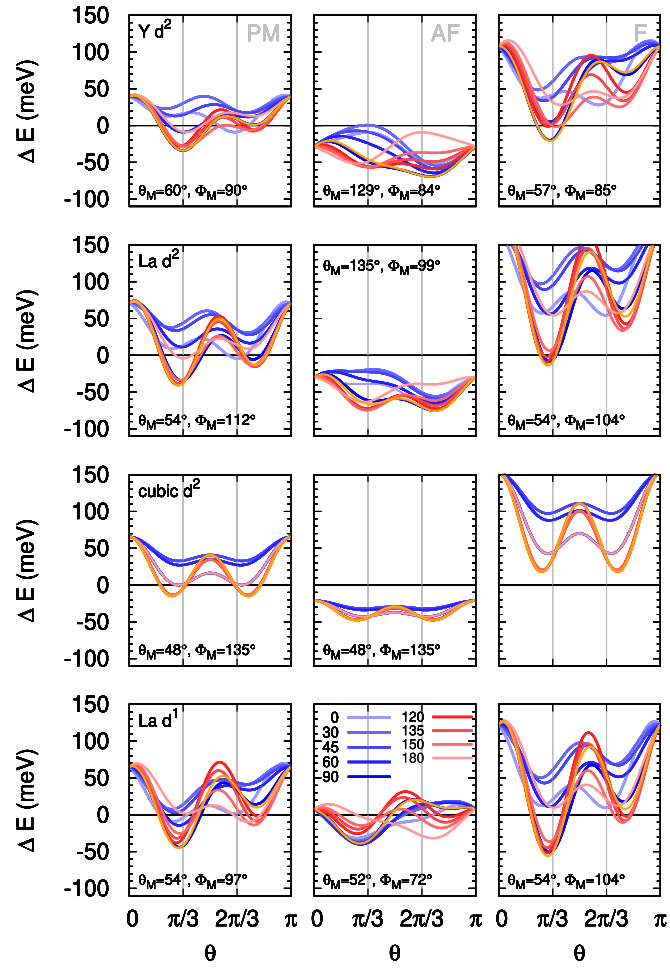

FIG. 3. Total superexchange energy gain for YVO_3 (top panel) and $LaVO_3$ (second panel from the top) in the para-(PM), antiferro-(AF), and ferromagnetic (F) case, $GdFeO_3$-type structure. Lines: different ϕ values in the $(0, \pi)$ interval, see the caption. Orange curve: ϕ_M, yielding the minimum. Third panel from the top: cubic case. Bottom panel: energy gain for the hopping integrals of $LaVO_3$, but in a hypothetical t_{2g}^1 configuration.

minimizing $\Delta E(\theta, \phi)$ yield $|\theta, \phi\rangle_{KK}$, the state obtained in LDA+DMFT calculations in the zero CF limit. The maximum quadratic SE energy gain, $|\Delta E(\theta_M, \phi_M)|$, increases from ~ 35 meV for YVO_3 to ~ 41 meV for $LaVO_3$, to ~ 46 meV for $LaTiO_3$ and $YTiO_3$, explaining the progressive increase in T_{KK} obtained in the DMFT calculations.

Figure 4 shows the various contributions to $\Delta E(\theta_M, \phi_M)$. The most important are the quadratic SE terms, those which can lead to a transition. For YVO_3 several channels have comparable weight—similar to the titanates [34]. In contrast, for $LaVO_3$, a single term, the $\hat{\tau}_i^{2,xz} \hat{\tau}_j^{2,xz}$ interaction, dominates, as in the cubic limit; the total energy gain from quadratic SE terms is, however, significantly larger than in the cubic limit since small positive and negative contributions cancel out.

The linear orbital Zeeman terms [34], whereas not giving rise to a phase transition, can generate a finite polarization tail already for $T > T_{KK}$ [12], which can either assist or hinder the transition. For the titanates there is a sizable tail in the $p_{KK}(T)$ curves in Fig. 2; furthermore, the linear terms

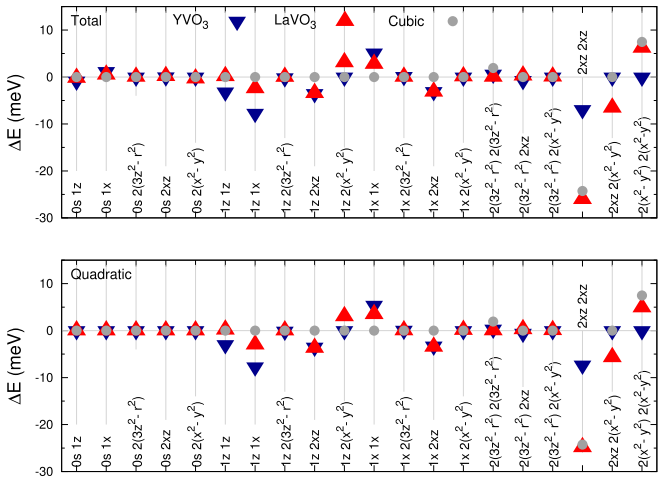

FIG. 4. Decomposition of $\Delta E(\theta,\phi)$ at the angles (θ_M,ϕ_M) that yield the absolute minimum in the paramagnetic case. Top: result from the total $\Delta E(\theta,\phi)$. Bottom: only quadratic terms are included. The components are specified on the horizontal axis; missing nondiagonal terms can be obtained via the transformation $r\mu \leftrightarrow r'\mu'$.

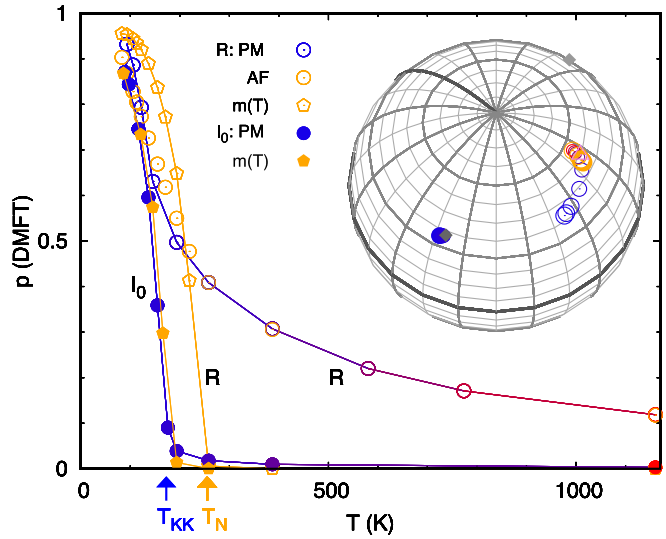

FIG. 5. $LaVO_3$, orbital and magnetic transition. Circles: orbital polarization. Pentagons: magnetization. Empty symbols: DMFT for experimental structure (R). Full symbols: DMFT for an ideal structure without CF splitting (I_0). Triangle: LDA. Rhombi: angles yielding the maximum SE energy-gain (AF case), obtained from quadratic terms (dark gray), and linear terms (light gray) only.

cooperate with the quadratic terms, favoring the occupation of the same orbital. For the vanadates, instead, the tail is negligible. The suppression of the orbital Zeeman effect turns out to be due to filling rather than to the band structure: Assuming identical hopping integrals in the two families of compounds, $D^{ij\,00}_{00,r\mu}(n=1)/D^{ij\,00}_{00,r\mu}(n=2)=\mathcal{W}_1/\mathcal{V}_1$ as defined in Ref. [35], Table III; the right-hand side depends only on J/U. The prefactor $\mathcal{W}_1$ for the t_{2g}^1 configuration can be sizably larger than the corresponding $\mathcal{V}_1$ for the t_{2g}^2 case—up to a factor of 10 for realistic J/U values [35]. This can be seen comparing the La d^2 and d^1 panels in Fig. 2.

Summarizing, in the PM phase, quadratic SE interactions are weaker in the vanadates than in the titanates, and the orbital Zeeman terms are negligible. $LaVO_3$ is, however, characterized by a very small CF splitting; the KK Hamiltonian form is close to the cubic limit, but the distortions actually increase the energy gained from ordering the orbitals. This makes $LaVO_3$ unique and results in low-temperature orbital physics being controlled by superexchange interactions.

IV. ORBITAL ORDERING AND THE *G*-TYPE ANTIFERROMAGNETIC PHASE

To obtain the final confirmation of the dominant role of superexchange in $LaVO_3$ we perform calculations allowing for G-type antiferromagnetism. For conventional orbitally ordered materials, where OO is driven by the Coulomb-enhanced crystal-field, $T_N \ll T_{OO}$. In $LaVO_3$, instead, we find that T_N and T_{OO} are comparable. In fact, as illustrated in Fig. 5, the magnetic ordering happens already *above* the orbital ordering transition, $T_N > T_{OO} \sim T_{KK}$. To explain this remarkable result, we return to the SE energy surfaces in Fig. 3, and compare the PM case, left column, to the AF case, center column. The figure shows that the AF curves are shifted uniformly downwards. This is due to the paraorbital ($r=0$) term with spin rank $q=1$; comparing to the bottom row of the figure, one may see that the latter is much larger in the t_{2g}^2 than in the t_{2g}^1 configuration. Furthermore, the quadratic energy gain for orbital ordering alone (obtained subtracting the paraorbital term) decreases going from the PM to the AF case; at the same time, the orbital Zeeman linear terms increase in importance but favor $\phi_{M'} \sim \phi_M + 180°$, hence, competing with the quadratic terms. Thus, at a given finite temperature with respect to the PM case, the OO hole orbital (orange open circle on the sphere) remains closer to the highest-energy CF orbital (triangle). Importantly, we obtain such a behavior only for $LaVO_3$; in the case of YVO_3, for the experimental structure we do not find any magnetic phase above T_{str} or T_{KK}, in line with experiments.

V. CONCLUSION

In conclusion, we have identified orthorhombic $LaVO_3$ as a rare case of a system hosting a Kugel'-Khomskii orbital-ordering transition. The relevance of SE in t_{2g}^2 vanadates has been previously suggested based on idealized model calculations [25], however, within a strong xz/yz-fluctuations picture. In fact, we have shown that orbital fluctuations, large at room temperature, are suppressed when approaching T_{str}. Furthermore, we have shown that SE is key only for $LaVO_3$. In all other cases considered, the conventional picture of the Coulomb-enhanced CF splitting applies. This is further confirmed by the fact that $T_N \sim T_{OO}$ only in orthorhombic $LaVO_3$. More strikingly, we find that $T_N > T_{KK} \sim T_{OO}$, opposite to what happens in conventional OO materials. Taking into account that DMFT as all mean-field theories somewhat overestimates ordering temperatures, our results provide a natural explanation for the proposed picture of orbital order and weak G-type magnetism (or short-range spin-orbital order) right above the structural orthorhombic-to-monoclinic transition [22–24].

ACKNOWLEDGMENTS

We would like to acknowledge computational time on JURECA and the RWTH-Aachen cluster via JARA, which was used for the actual computations, as well as computational time on JUWELS, which was used for code development.

[1] K. I. Kugel' and D. I. Khomskii, Zh. Eksp. Teor. Fiz. **64**, 1429 (1973) [Sov. Phys. JETP **37**, 725 (1973)].

[2] J. Kanamori, J. Appl. Phys. **31**, S14 (1960).

[3] D. I. Khomskii, *Transition Metal Compounds* (Cambridge University Press, Cambridge, UK, 2014), p. 204.

[4] A. I. Liechtenstein, V. I. Anisimov, and J. Zaanen, Phys. Rev. B **52**, R5467 (1995).

[5] Y. Tokura and N. Nagaosa, Science **288**, 462 (2000).

[6] P. Fazekas, *Lecture Notes on Electron Correlation and Magnetism* (World Scientific, Singapore, 1999).

[7] E. Pavarini, E. Koch, and A. I. Lichtenstein, Phys. Rev. Lett. **101**, 266405 (2008).

[8] E. Pavarini and E. Koch, Phys. Rev. Lett. **104**, 086402 (2010).

[9] C. Autieri, E. Koch, and E. Pavarini, Phys. Rev. B **89**, 155109 (2014).

[10] A. Flesch, E. Gorelov, E. Koch, and E. Pavarini, Phys. Rev. B **87**, 195141 (2013).

[11] A. Flesch, G. Zhang, E. Koch, and E. Pavarini, Phys. Rev. B **85**, 035124 (2012).

[12] J. Musshoff, G. R. Zhang, E. Koch, and E. Pavarini, Phys. Rev. B **100**, 045116 (2019).

[13] H. Sims, E. Pavarini, and E. Koch, Phys. Rev. B **96**, 054107 (2017).

[14] E. Pavarini, S. Biermann, A. Poteryaev, A. I. Lichtenstein, A. Georges, and O. K. Andersen, Phys. Rev. Lett. **92**, 176403 (2004).

[15] E. Pavarini, A. Yamasaki, J. Nuss, and O. K. Andersen, New J. Phys. **7**, 188 (2005).

[16] M. De Raychaudhury, E. Pavarini, and O. K. Andersen, Phys. Rev. Lett. **99**, 126402 (2007).

[17] X.-J. Zhang, E. Koch, and E. Pavarini, Phys. Rev. B **102**, 035113 (2020). In Fig. 4 of this paper, the highest temperature $p(T)$ values for the real structure have been swapped by mistake with those for a larger crystal field, see X.-J. Zhang, E. Koch, and E. Pavarini, Phys. Rev. B **105**, 159904(E) (2022).

[18] P. Bordet, C. Chaillout, M. Marezio, Q. Huang, A. Santoro, S-W. Cheong, H. Takagi, C. S. Oglesby, and B. Batlogg, J. Solid State Chem. **106**, 253 (1993).

[19] S. Miyasaka, Y. Okimoto, M. Iwama, and Y. Tokura, Phys. Rev. B **68**, 100406(R) (2003).

[20] J.-Q. Yan, J. S. Zhou, and J. B. Goodenough, Phys. Rev. Lett. **93**, 235901 (2004).

[21] J.-Q. Yan, J.-S. Zhou, J. G. Cheng, J. B. Goodenough, Y. Ren, A. Llobet, and R. J. McQueeney, Phys. Rev. B **84**, 214405 (2011).

[22] Y. Ren, A. A. Nugroho, A. A. Menovsky, J. Strempfer and U. Rütt, F. Iga and T. Takabatake, C. W. Kimball, Phys. Rev. B **67**, 014107 (2003).

[23] J.-S. Zhou, Y. Ren, J.-Q. Yan, J. F. Mitchell, and J. B. Goodenough, Phys. Rev. Lett. **100**, 046401 (2008).

[24] L. D. Tung, A. Ivanov, J. Schefer, M. R. Lees, G. Balakrishnan, and D. McK. Paul, Phys. Rev. B **78**, 054416 (2008).

[25] G. Khaliullin, P. Horsch, and A. M. Oleś, Phys. Rev. Lett. **86**, 3879 (2001).

[26] *DMFT: From Infinite Dimensions to Real Materials Modeling and Simulation*, edited by E. Pavarini, E. Koch, A. Lichtenstein, and D. Vollhardt (Verlag des Forschungszentrum Jülich, Jülich, Germany 2018), Vol. 8, and references within.

[27] The small spin-orbit coupling and related entanglement effects are neglected.

[28] P. Blaha, K. Schwarz, P. Sorantin, and S. Trickey, Comput. Phys. Commun. **59**, 399 (1990).

[29] N. Marzari and D. Vanderbilt, Phys. Rev. B **56**, 12847 (1997).

[30] A. A. Mostofi, J. R. Yates, Y.-S. Lee, I. Souza, D. Vanderbilt, and N. Marzari, Comput. Phys. Commun. **178**, 685 (2008); J. Kuneš, R. Arita, P. Wissgott, A. Toschi, H. Ikeda, and K. Held, *ibid.* **181**, 1888 (2010).

[31] T. Mizokawa and A. Fujimori, Phys. Rev. B **54**, 5368 (1996).

[32] E. Gull, A. J. Millis, A. I. Lichtenstein, A. N. Rubtsov, M. Troyer, and P. Werner, Rev. Mod. Phys. **83**, 349 (2011).

[33] J. Mußhoff, A. Kiani, and E. Pavarini, Phys. Rev. B **103**, 075136 (2021).

[34] See Supplemental Material at http://link.aps.org/supplemental/10.1103/PhysRevB.106.115110 for more details.

[35] X.-J. Zhang, E. Koch, and E. Pavarini, Phys. Rev. B **105**, 115104 (2022).